ADVANCED FUNCTIONAL MATERIALS

FULL PAPER

DOI: 10.1002/adfm.200701478

Efficient TiO_2 Photocatalysts from Surface Hybridization of TiO_2 Particles with Graphite-like Carbon**

By *Li-Wu Zhang, Hong-Bo Fu,* and *Yong-Fa Zhu**

Surface hybridization of TiO_2 with graphite-like carbon layers of a few molecular layers thickness yields efficient photocatalysts. Photoelectrochemical measurements confirm an electronic interaction between TiO_2 and the graphite-like carbon. A TiO_2 photocatalyst with a carbon shell of three molecular layers thickness (~1 nm) shows the highest photocatalytic activity which is about two times higher than that of Degussa P25 TiO_2 under UV light irradiation. The mechanism of the enhanced photocatalytic activity under UV irradiation is based on the high migration efficiency of photoinduced electrons at the graphite-like carbon/TiO_2 interface, which is due to the electronic interaction between both materials. In addition, a high activity under visible light irradiation is observed after graphite-like carbon hybridization. TiO_2's response is extended into the visible range of the solar spectrum due to the electronic coupling of π states of the graphite-like carbon and conduction band states of TiO_2.

1. Introduction

In recent years, the photocatalytic degradation of organic compounds has attracted much attention due to its potential to purify wastewater that is discharged from industry and households.[1] Heterogeneous photocatalysts offer great potential for converting photon energy into chemical energy and therefore decomposing organic contaminants. A typical example is the TiO_2-based photocatalytic detoxification of air and water for environmental remediation.[2] However, there are still many challenges remaining that are yet to be met before these photocatalytic processes become economically feasible. Difficulties include the enhancement of solar energy conversion and the supression of the recombination of photogenerated electron-hole pairs.

Several methods have been developed to increase the efficiency of the photocatalytic process of TiO_2. One approach is doping, which introduces additional states in the TiO_2 bandgap and thereby increases visible light absorbance. Anion doping with N, C, and S ions or transition-metal cation doping is commonly used to convert TiO_2 into a visible-light photocatalyst.[3] However, the fact that the states introduced act as combining centers for electron-hole pairs as well as the thermal instability associated with doped materials gave rise to some doubts about their performance.[3,4] Another approach to increase the efficiency is coating, e.g., noble metal coating,[5] semiconductor coating,[6] dye coating,[7] and many more. Metal coating enhances the efficiency of the interfacial charge-transfer process through the formation of a ''Schottky'' barrier between metal and TiO_2, which can be attributed to the different Fermi levels of the metal and the TiO_2.[3,4] In the case of semiconductor coating, the synergy of the coupled semiconductors improves the charge separation in the photocarrier generation process. For all coating methods, the electronic interaction between TiO_2 and coating material(s) plays an import role in the eventual photocatalytic performance of the composite. With the development of new methods for the modification of TiO_2 new types of electronic interactions have been introduced into TiO_2 photocatalysts, e.g., by combining *p*-type and *n*-type semiconductors, diode photocatalysts with *p-n* junctions at the interface were designed, which are able to efficiently separate electron-hole pairs,[8] and by formation of an electronic interaction of TiO_2 and a with small band-gap oxide such as Fe_2O_3, photocatalysts that are sensitized to visible light were realized,[9] and lastly splitting of pure water was achieved with a dye-coated photocatalysts which is attributed to the electronic contact between dye and photocatalyst.[7] Therefore, the development of novel methods for the modification of TiO_2 in view of new electronic interactions is significant and meaningful.

Conjugated materials are a category of materials with unique properties in electron or hole transport.[10] We propose that these conjugated materials are excellent candidates for improving the transport of photocarriers during photocatalysis through the formation of electronic interactions with TiO_2. To the best of our knowledge, few efforts have been made to electronically combine conjugated materials with photocatalysts. Graphite has a conjugated structure and although the preparation of graphite coated TiO_2 and a

[*] Prof. Y.-F. Zhu, Dr. L.-W. Zhang
Department of Chemistry, Tsinghua University
Beijing, 100084 (PR China)
E-mail: zhuyf@mail.tsinghua.edu.cn
Prof. H.-B. Fu
Department of Environment Science and Engineering
Fudan University Shanghai, 200433 (PR China)

[**] This work was partly supported by the Chinese National Science Foundation (20673065) and the National Basic Research Program of China (2007CB613303). Supporting Information is available online from Wiley InterScience or from the author.

ADVANCED FUNCTIONAL MATERIALS

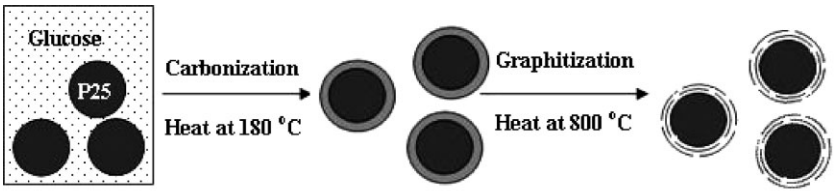

Scheme 1. Synthetic procedure for the preparation of graphite-encapsulated TiO_2.

subsequently enhanced photocatalytic activity were reported recently,[11] and carbon-modified TiO_2 has been described extensively in the literature,[12] hardly any attention has been paid to the analysis of the electronic interaction between graphitic carbon and TiO_2. Herein, we present a simple method to hybridize TiO_2 with graphite-like carbon layers. The electronic interaction between TiO_2 and graphite-like carbon as well as the resulting effects on the photocatalytic activity of the TiO_2 photocatalyst were investigated systematically.

2. Results and Discussion

2.1. Structure and Morphology of TiO_2/Carbon Nanoparticles

In the current work, the encapsulation of TiO_2 with graphite-like carbon was realized with a two step process (Scheme 1). The first step involves the fabrication of TiO_2/carbon core-shell structures through a hydrothermal method at 180 °C, using commercial P25 TiO_2 and glucose as starting materials. The shell thickness is tunable by simply increasing or decreasing the glucose content. Then, graphitization of the carbonaceous cages is achieved by calcination which is conducted in a tube furnace at 800 °C for 3 h in a N_2 gas atmosphere.

An estimate of the carbon content in the TiO_2/carbon core-shell nanoparticles was obtained by thermogravimetric analysis (TGA). In all the samples no weight loss was observed until 500 °C. Major weight loss commenced at 500 °C and was completed at 650 °C, which can be attributed to the oxidation of carbon. The carbon content of the samples increased with increasing mass ratio of glucose and TiO_2 during hydrothermal treatment, and is therefore easily controlled by changing the. For example, the carbon content of sample GT05-800 was calculated to be approximately 5.4 wt% (see supporting information). As displayed in Table 1, the thickness of the carbon shell also increases with an increase in glucose:TiO_2 mass ratio.

Figures 1a and 1b show the X-ray diffraction (XRD) patterns of GT products prepared at different temperatures and with different mass ratios of glucose and TiO_2, respectively. Figure 1a illustrates that GT05-500, GT05-700, and GT05-800 are all composed of a mixture of anatase and rutile TiO_2 – nearly the same crystal composition as P25 TiO_2. It is known that the phase transformation from anatase to rutile occurs at around 600 °C.[13] However, in the present study we observed that the anatase phase in graphite-like carbon modified P25 TiO_2 is sustained even above this temperature. Obviously, the presence of carbon on the surface of the titania inhibits its phase transformation, leading to a higher thermal stability. GT samples with different carbon content were prepared at 800 °C, and their XRD patterns are shown in Figure 1b. P25-800 was prepared by direct calcination of P25 TiO_2 at 800 °C without carbon encapsulation. It is observed that nearly all the anatase phase was transformed into rutile at this temperature. A similar result was found for sample GT02-800, which had a very small carbon content (about 3 wt%). Upon increasing the carbon content more of the anatase phase was preserved. The crystal composition of each sample is given in Table 1. Samples GT04-800, GT05-800, and GT10-800 retained a similar crystal composition to the starting material, P25, which suggests a possible phase transfer suppression effect of the carbon shells. The carbon shells are acting as barriers for the phase transformation from anatase to rutile. It can be speculated that the high energy introduced into the system through the high temperature is directly exposed to the carbon shells and not the TiO_2 core; thus, the core retains the anatase phase. Average crystal sizes were calculated via the Scherrer equation using the position of the (101) peak in the XRD spectrum. It was found that samples which exhibited the same crystal composition as P25 essentially also exhibited the same crystal size as P25, demonstrating that the encapsulation of carbon

Table 1. Physicochemical characterization of GT and P25 samples.

sample	mass ratio of glucose and TiO_2 [%]	carbon shell thickness [nm]	degree of graphitization $I_{D\text{-}band}/I_{G\text{-}band}$ [a.u.]	S_{BET} ($m^2 \cdot g^{-1}$)	crystal phase(s)
P25 TiO_2	0	0	–	45.2	A 80% R 20%[a]
P25-800	0	0	–		R
GT01-800	20	0–1	0.87	36.1	R
GT03-800	43	0–1	0.84	46.4	A 70% R 30%
GT05-800	55	1–2	0.94	51.2	A 80% R 20%
GT07-800	64	3	–	52.2	A 80% R 20%
GT08-800	66	3–4	1.01	67.6	A 80% R 20%
GT10-800	72	5	1.18	75.8	A 80% R 20%

[a]A = anatase TiO_2; R = rutile TiO_2.

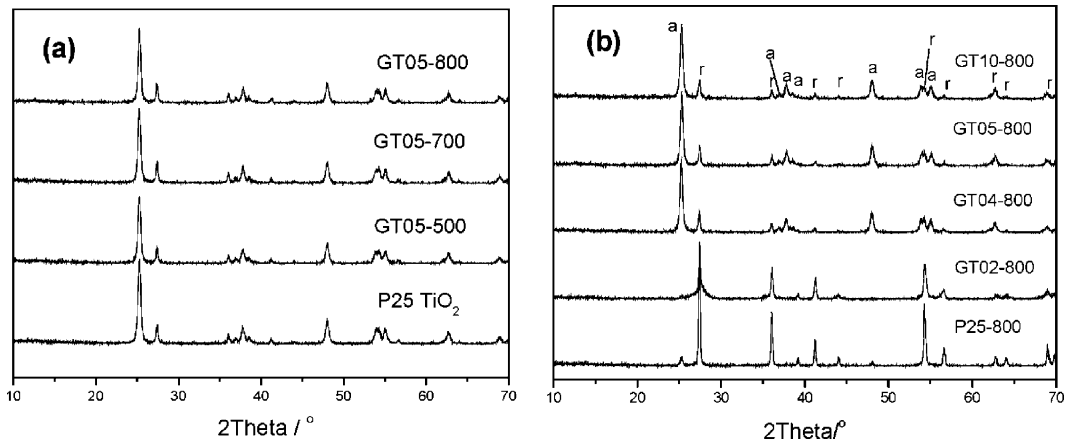

Figure 1. X-ray diffraction (XRD) patterns of GT products prepared at: a) different temperatures and b) using a range of mass ratios of glucose and TiO_2 during synthesis. [a = anatase phase, r = rutile].

layers also suppresses crystal growth of TiO_2 even when undergoing high temperature calcination.

Figure 2 shows transmission electron microscopy (TEM) images of GT composites prepared with different mass ratios of glucose and TiO_2 during the hydrothermal process. As can be seen from the images, the TiO_2 particles are surrounded by carbon shells. Figure 2a shows a TEM image of GT05-800, which is prepared with 0.5 g glucose. The carbon shell is not visible at this resolution, but a high-resolution (HR) TEM image (Fig. 5) shows the carbon layer is ~1 nm. The sample prepared with 1.0 g glucose (GT10-800) had a carbon shell of ~5 nm thickness, whereas one with more glucose added (2.0 g) showed a ~7 nm thick carbon shell. Hence, the thickness of the carbonaceous sheaths increases with increasing glucose:TiO_2 mass ratio. This is because more carbon is formed during the hydrothermal process when a higher concentration of glucose is present in the starting mixture under otherwise identical experimental conditions. In addition, the TiO_2 core in these samples was of essentially the same size for all samples, which is in accordance with the XRD results.

Figure 3 shows the Raman spectra of TiO_2/carbon core-shell nanoparticles in comparison with that of pure P25 TiO_2. According to the symmetry group analysis, anatase TiO_2 has 15 optical modes in Raman (the irreducible representation $1A_{1g} + 1A_{2u} + 2B_{1g} + 1B_{2u} + 3E_g + 2E_u$). Modes A_{1g} (519 cm^{-1}), B_{1g} (399 and 519 cm^{-1}), and E_g (144, 197, and 639 cm^{-1}) are Raman-active modes of anatase and thus six fundamental transitions are expected in the Raman spectrum of anatase.[14] Meanwhile, the four modes A_{1g} (612 cm^{-1}), B_{1g} (143 cm^{-1}), B_{2g} (826 cm^{-1}), and E_g (447 cm^{-1}) are the Raman-active modes of rutile.[15] Peaks observed in the Raman spectra of the GT composites and P25 are similar to those of bulk anatase but with a slight shift. Compared with P25, the intensity of the peaks at 143 and 195 cm^{-1} is increased in the spectra of the GT samples, indicating an enhanced crystallinity. It was previously reported that a transition from anatase to rutile occurs at temperatures above 600 °C,[12] but no characteristic rutile peaks were observed in the spectra of the GT composites which were prepared at 800 °C. This observation suggests that the phase transformation from anatase to rutile was suppressed due to the presence of carbon inhibiting the formation of the rutile phase. Reportedly, the low-frequency peak at 144 cm^{-1} in the spectrum of anatase TiO_2 nanoparticles shows a strong dependence on quantum size confinement effects.[16] Several groups used phonon confinement models and stoichiometry of TiO_2 to correlate shift and width of the E_g anatase mode at 144 cm^{-1} with the crystalline domain size.[17,18] According to these reports, a blueshift of the E_g mode is expected with increasing particle size. Contrary to this, our results clearly show an obvious red-shift for the E_g mode (inset of Fig. 3) of GT composites even though they should have larger particle sizes than P25 due to the high calcination temperature. The Raman peak at 195 cm^{-1} was also shifted to longer wavenumbers, while the peaks at 395, 515, and 637 cm^{-1} were shifted to shorter wavenumbers. Raman spectroscopy is very sensitive to the crystallinity and microstructure of materials. Therefore, these shifts of the Raman peaks indicate that a close interaction might exist between carbon and TiO_2.

The nature of the carbon present in the GT samples was also investigated by Raman spectroscopy and the results are shown in Figure 4. All sample spectra show two peaks around 1341 and 1596 cm^{-1}. The Raman-active E_{2g} mode at 1596 cm^{-1} is characteristic for graphitic sheets and we were able to record well-defined *G*-bands for all our samples which confirms the presence of sp^2 carbon-type structures within the carbonaceous wall of the GT samples.[19] The *D*-band at around 1341 cm^{-1} can be attributed to the presence of defects within the hexagonal graphitic structure. Since the intensities of the *G*-bands are comparable to those of the *D*-bands, we conclude that the samples have some degree of atomic-scale ordering. Compared with the spectra of pure graphite crystals (1575 cm^{-1}), the *G*-band shifted to higher wavenumbers in all sample spectra, which suggests some structural imperfections of the carbon shells.[20,21] The intensity ratio of *D*- and *G*-band

ADVANCED FUNCTIONAL MATERIALS

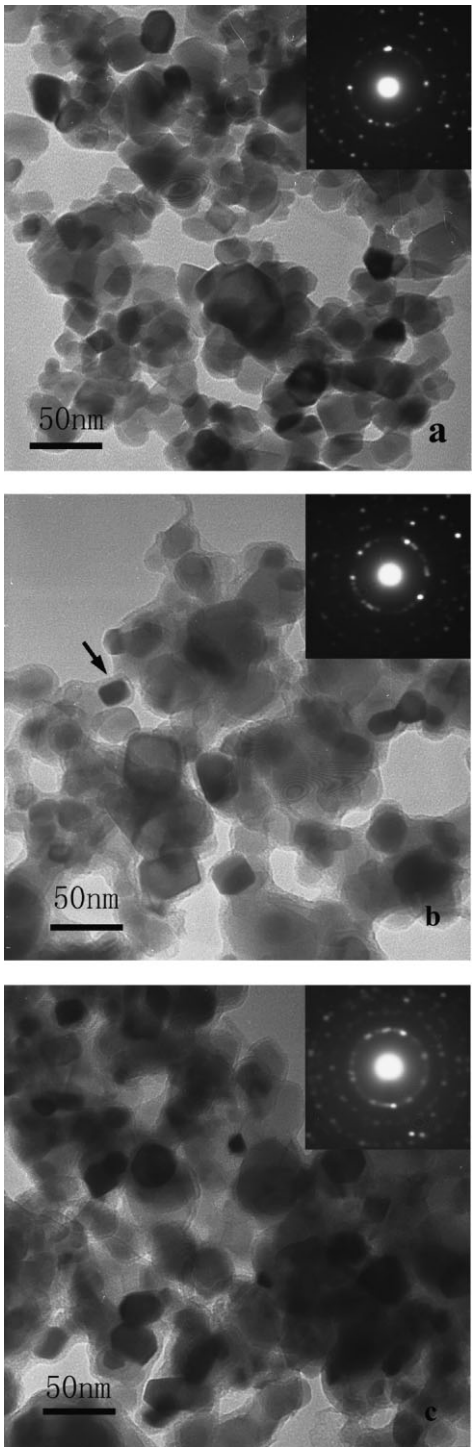

Figure 2. Transmission electron microscopy (TEM) images of GT composites prepared using various mass ratios of glucose and TiO_2 during synthesis. a) GT05-800, b) GT10-800, c) GT20-800.

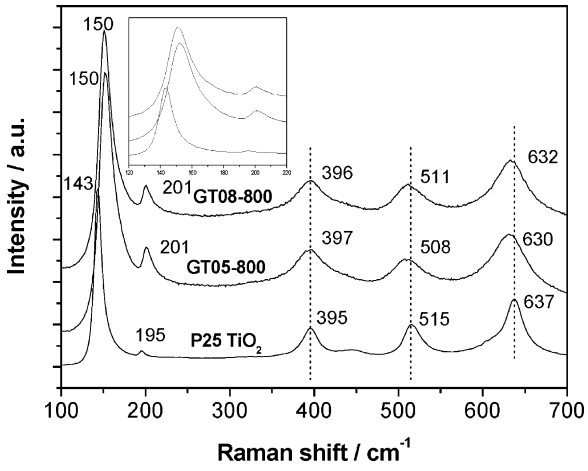

Figure 3. Raman spectra of GT composites and P25 TiO_2. Inset shows an expanded part of the spectra which ranges from 100–250 cm^{-1}.

($I_{D\text{-}band}/I_{G\text{-}band}$) is indicative of the degree of graphitization and its value for each sample is shown in Table 1. The ratio decreases with increasing carbon content, which indicates that samples with thinner carbon shells form a more ordered carbon structure during the graphitization process. The shift of *D*-band in the spectra of samples GT08-800 and GT10-800 to lower wave numbers, 1329 and 1315 cm^{-1}, respectively, could possibly be attributed to the relatively low ordered carbon structure.

Figure 5 shows high-resolution (HR) TEM images of sample GT05-800 which were used to estimate carbon shell thickness and TiO_2 nanoparticle size. The images show that the TiO_2 particles are surrounded by a few graphitic layers, and the overall thickness of the carbon shell is about 1 nm. The *d*-spacing of the graphitic layers is 0.34 nm, which is in agreement with the literature. As can be seen from the HRTEM images as well, there are still many defects within the

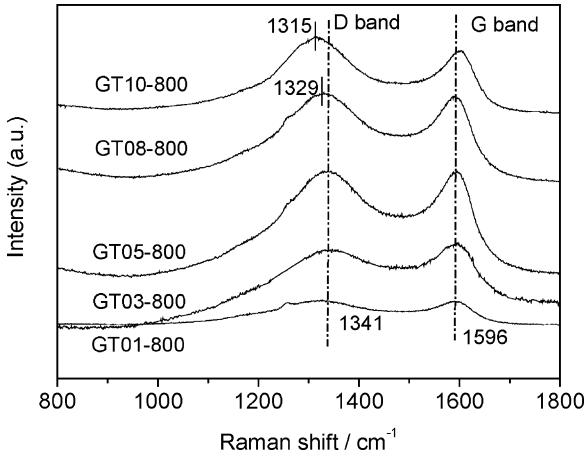

Figure 4. Raman spectra of GT samples exhibiting graphitic modes.

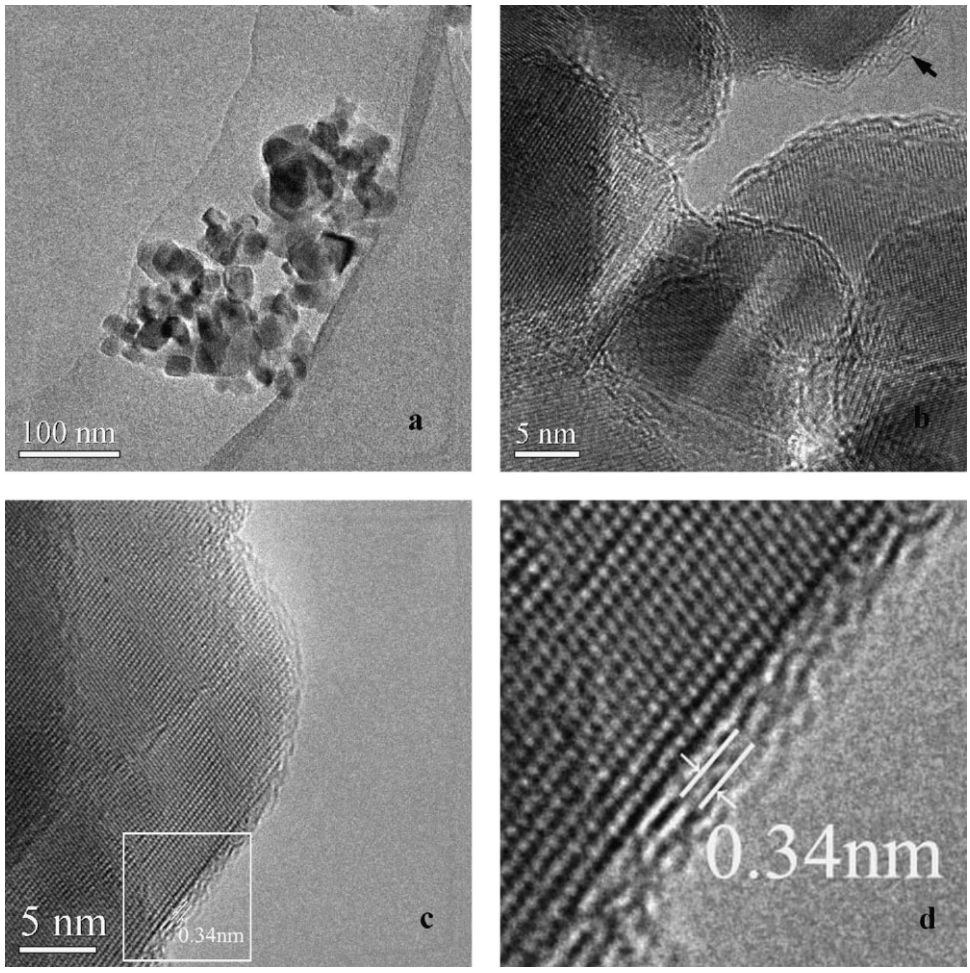

Figure 5. High-resolution (HR)-TEM images of sample GT05-800.

graphite layers, which is in good agreement with the Raman results. However, since the surface of the TiO_2 nanoparticles is fully covered with a thin graphite-like carbon film a good electronic contact between oxide semiconductor and carbon was achieved.

The optical properties of the GT samples were probed with UV-vis diffuse reflectance spectroscopy (Fig. 6). As expected, P25 shows the characteristic spectrum of TiO_2 with its fundamental absorption sharp edge rising at 400 nm, while the GT samples absorb in the visible light region due to the presence of carbon on the TiO_2 surface. The absorption edge of TiO_2 can also be detected in the spectra of the GT samples. The TiO_2 peak is not shifted for GT05, GT07, and GT10, indicating identical band gap energies. This is contrary to earlier reports where a decrease in band gap energy was observed for carbon-doped TiO_2 due to the substitutional nature of the incorporated carbon.[22] In the present work, most of the carbon in the GT samples was free, graphitic carbon, hence no change in band gap energy was observed and instead an intense, broad background absorption in the visible light region dominated the UV-vis spectra. It is notable that compared to P25 TiO_2, the absorption edge of GT01 and GT02 experienced a red-shift of about 20 nm, which may be due by the higher content of rutile in these samples, as rutile has a narrower band gap (3.0 eV) than anatase (3.2 eV). Additionally, it is noteworthy that there is an obvious correlation between carbon content and changes observed in the UV-vis spectrum of a sample. The UV-vis

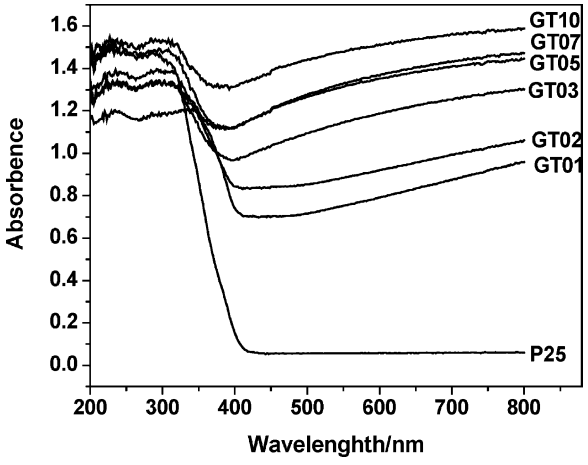

Figure 6. UV-vis diffuse reflection spectra of GT samples and P25 TiO_2.

absorption of the GT samples increases with increasing carbon content. This suggests an increased electric surface charge of the oxide within the composite due to the introduction of the carbon which can possibly cause modifications of the fundamental process of electron-hole pair formation during irradiation.

2.2. Photocatalytic Properties

The photoactivity of GT samples was evaluated by degradation of formaldehyde (FAD), a hazardous air pollutant as well as a common model compound to test the photodegradation capability of photocatalysts. Figure 7a shows time profiles of C/C_0 under UV irradiation, where C is the concentration of FAD at the irradiation time t and C_0 the concentration in the absorption equilibrium of the photocatalysts before irradiation. After 10 min irradiation with UV light about 85% of FAD were degraded in the presence of GT05-800, while approximately 20 min were required to reach the same level of degradation with P25 TiO_2. This confirmed the superiority of GT05-800 over P25 TiO_2 as was already expected from the photocurrent generation behavior. Apart from CO_2, which evolves through Equation 1, no intermediate reaction products were detected.

$$HCHO + O_2 \rightarrow CO_2 + H_2O \quad (1)$$

We calculated the average degradation rates for the photodecomposition of FAD according to Equation 2. Values of the average rate of FAD degradation for each sample are plotted in Figure 7b.

$$k = \frac{(C_0 - C)}{t} \quad (2)$$

Out of all samples, GT05-800 had the highest photocatalytic activity for FAD decomposition. GT03-800, GT04-800, GT06-800, and GT07-800 exhibited a higher activity than P25, while GT01-800, GT02-800, and GT08-800 were less active.

The photoactivity of GT05-800 was also evaluated in the visible light range of the spectrum ($\lambda > 420$ nm). Again photodegradation of FAD was used as measurement tool. Figure 8 shows the time profiles of $\ln(C/C_0)$ for GT05-800 and P25 under visible light irradiation. AS obvious from the graph a first-order linear relationship was revealed by the plots of $\ln(C/C_0)$ vs. irradiation time. P25 TiO_2 exhibited negligible degradation of FAD, while GT05-800 was photoactive with the reaction constant k being estimated to be 0.0049 min^{-1}. Blank (no photocatalyst) and dark (no irradiation) experiments were also performed, but hardly any FAD was decomposed and no CO_2 was detected in either case.

2.3. Mechanism of Photocatalytic Activity Enhancement

The photocatalytic activity of semiconductor oxides is mainly governed by surface area, crystallinity, and adsorption ability. Crystal formation significantly affected the photocatalytic activity of our GT samples. At lower carbon contents the transformation of anatase to rutile is not efficiently suppressed during the graphitization process. Consequently, GT01-800 and GT02-800 both showed lower activity than pure P25 TiO_2. As the carbon loading increases the phase transformation is more and more suppressed. The crystal composition data listed in Table 1 shows that a transformation of anatase to rutile occurs during calcination of GT03-800 and GT04-800, but the transformation is efficiently suppressed for GT05-800 (carbon content 5.4 wt%). We can therefore conclude that the minimum amount of carbon that is required for suppression of the phase transformation is approximately 5.4 wt%, which is consistent with results (5 wt%) reported by Inagaki et al.[23] It is thus understandable that the photocatalytic activity of GT05-800 is much higher than that of GT04-800. Interestingly, sample GT08-800, with a perfectly sustained anatase phase, also showed a lower activity than P25 TiO_2. This decreased activity at higher carbon contents is attributed to increased absorbance and scattering of photons through excess carbon in the photosystem. Too much graphite coating can therefore shield the light from reaching the surface

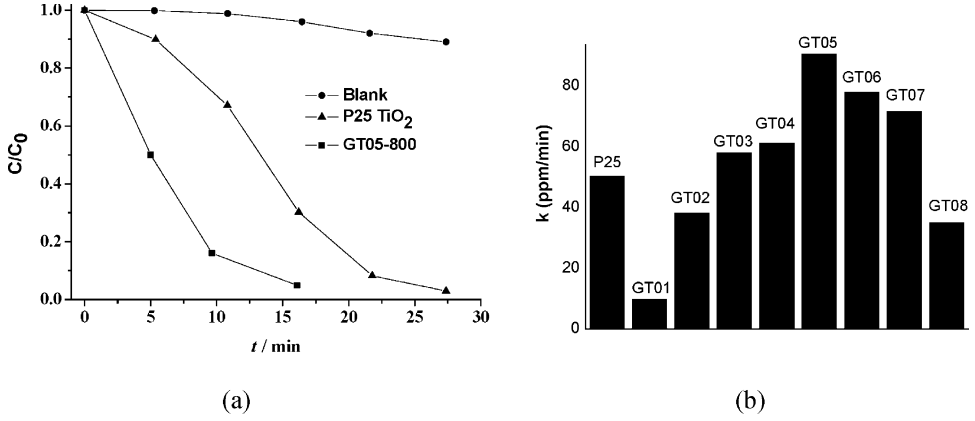

Figure 7. a) Formaldehyde (FAD) decomposition upon UV irradiation. b) Average degradation rates for the photodecomposition of FAD with P25 TiO_2 and various GT samples prepared with different amounts of glucose.

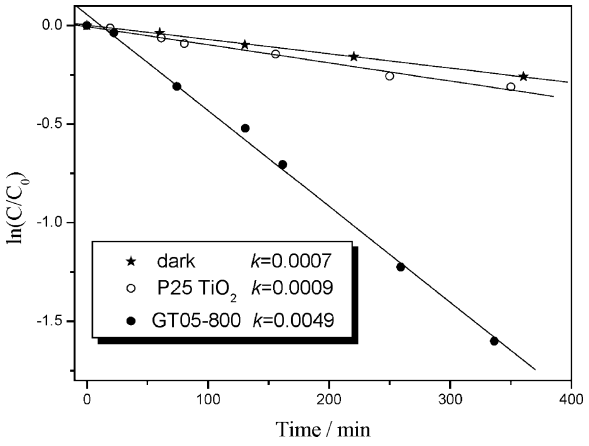

Figure 8. FAD decomposition upon visible light irradiation ($\lambda > 420$ nm). The average light intensity was 31.4 mW · cm^{-2}.

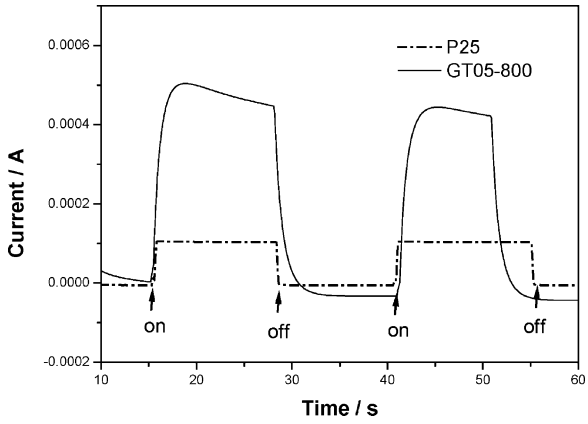

Figure 9. Photoelectrochemical responses of GT05-800 and P25 TiO_2 electrodes. [Na_2SO_4] = 0.5 M. Input power = 37.6 μW · cm^{-2}.

of the TiO_2 photocatalyst. However, carbon coating had some advantages, such as the suppression of the phase transition from anatase to rutile and the efficient separation of electron-hole pairs. In order to achieve a high photodecomposition rate, a balance between these different effects of the graphite layers is required. Sample GT05-800 (carbon content of about 5.4 wt%) gave the highest rate constant in the present work while the transition to rutile was suppressed and the graphite shell was thin enough to transmit light to the surface of the TiO_2 particle.

In this work, GT03-800, GT04-800, GT06-800, and GT07-800 all showed higher activity than pristine P25. An improved adsorption of FAD after carbon coating might also be one of the reasons for the increased activity. However, BET studies found that the GT composites exhibited a similar surface area like P25 TiO_2 and FAD absorption measurements showed that no obvious improvement in the adsorption of FAD was achieved (see Supporting Information), except for GT08-800, which had much higher surface area and capacity for FAD adsorption. Surprisingly GT05-800 also showed activity for FAD decomposition under visible light irradiation. The close interaction between graphite-like carbon and TiO_2 is thus considered to be an important factor affecting the photocatalytic activity of TiO_2. Hence, Mott-Schottky-(MS) measurements also known as photocurrent measurements were performed to investigate the electronic interaction of graphite-like carbon and TiO_2.

Photocurrent measurements were carried out for GT05-800 and P25 TiO2 after deposition on ITO electrodes (Fig. 9). The potential of the working electrode against a Pt counter electrode was set at 0.0 V. A fast and uniform photocurrent response was observed for each switch-on and switch-off event in both electrodes (GT05-800 and P25 TiO_2). This photoresponsive phenomenon was entirely reversibe. The photocurrent of the GT05-800 electrode was about four times as high as that of the P25 TiO_2 electrode which indicates that the separation efficiency of photoinduced electrons and holes was improved through the electronic interaction between graphite-like carbon and TiO_2.

Figure 10 shows electrochemical impedance spectroscopy (EIS) Nynquist plots of P25 TiO_2 and GT05-800 electrodes before and after UV irradiation. The diameter of the arc radius on the EIS Nynquist plot of the GT05-800 electrode is smaller than that of the P25 TiO_2 electrode regardless of whether with or without UV irradiation. The smaller the arc radius of a EIS Nynquist plot the higher the efficiency of charge separation. Thus, in the case of GT05-800 the photoinduced electron-hole pairs are easier separated and transferred to the sample surface which is due to the modification of the sample with graphite-like carbon, i.e., the photoinduced electrons and holes are separated more efficiently through an interfacial interaction between graphite-like carbon and TiO_2.

In order to better understand the differences in the electronic properties of P25 materials with and without graphite-like carbon layer coating, Mott-Sckottky (MS) measurements

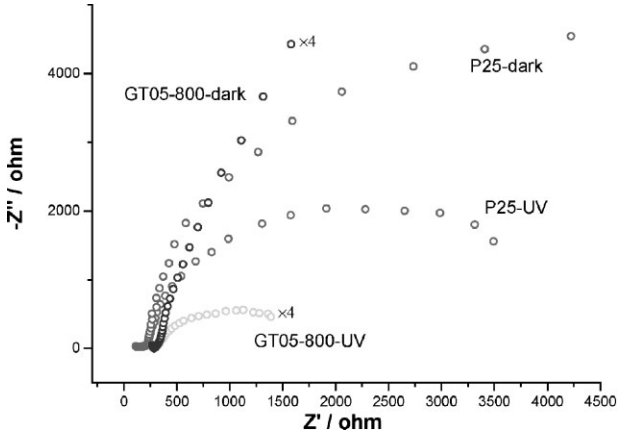

Figure 10. Electrochemical impedance spectroscopy (EIS) Nynquist plots of P25 TiO_2 and GT05-800 electrodes before and after UV irradiation. For better comparison the EIS Nynquist plot of GT05-800 is shown with four times magnification.

were also performed in darkness using impedance techniques.[24] Figure 11 shows MS plots of electrodes based on sintered P25 and GT05-800. Reversed sigmoidal plots were observed with an overall shape that is consistent with that of typical *n*-type semiconductors. The flat-band potentials, as calculated from the x intercepts of the linear region, were found to be -0.22 and 0.08 V vs. Ag/AgCl for P25 and GT05-800, respectively. GT05-800 experienced a large positive shift of the flat-band potential when compared with pristine P25. Additionally, the slope of the linear region for the P25 electrode is lower in value, which suggests a higher donor density.

Photocurrent action spectra were collected in order to examine the effect of graphite-like carbon films on the photoelectrochemical properties of TiO_2. The results for both P25 TiO_2 and GT05-800 are shown in Figure 12. The P25 electrode showed a maximum photocurrent in the UV range that is located at 330 nm, while no photocurrent was generated under visible light irradiation. Interestingly, the GT05-800 electrode showed a broad but much more intense photocurrent peak covering the range from 320 to 450 nm, thus extending into the visible light range. Its maximum signal appeared at 350 nm, 20 nm red-shifted from that of P25 TiO_2.

Based on the above results, the electronic interaction between graphite-like carbon layer and TiO_2 is confirmed and the enhanced photocatalytic activity can be explained in the following way: Photo-generated electrons and holes within the TiO_2 particles either take part in redox reactions at the surface or recombine. The recombination process has a faster kinetics than the redox reactions and therefore controls the efficiency of the photocatalytic process.[25] In the presence of graphite-like carbon, photo-generated electrons are scavenged by graphite-like carbon layers. Thus, the possibility of the recombination of e^-/h^+ pairs decreases. Meanwhile, O_2 absorbed on the surface of the graphite-like carbon layers can accept e^- and form $\cdot O_2^-$ which then oxidizes FAD directly on the surface. This mechanism of the enhancement of the photocatalytic activity is illustrated in Scheme 2.

While the bandgap energy of GT05-800 is nearly the same as that of P25 TiO_2, the flat-band potential of GT05-800 is shifted

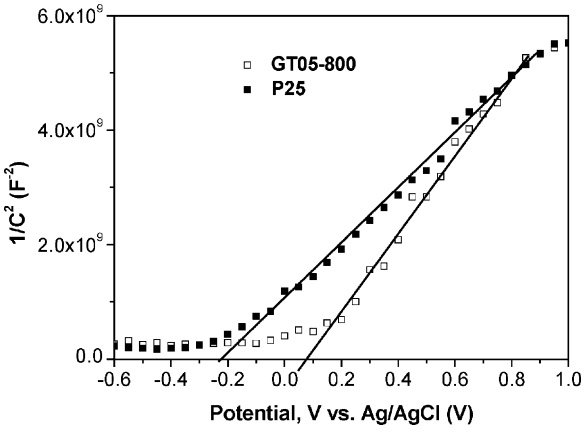

Figure 11. Mott-Schottky (MS) plots of P25 and GT05-800 thin film electrodes.

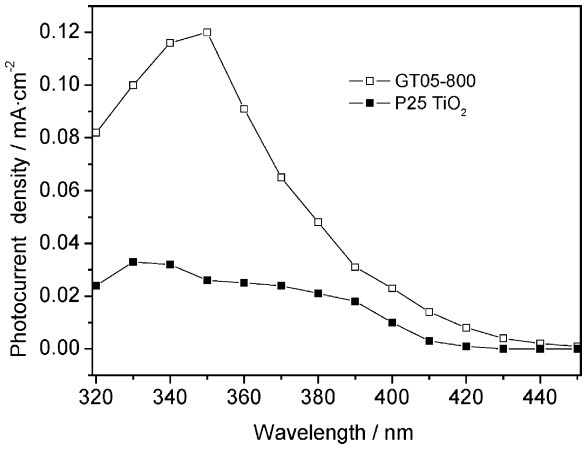

Figure 12. Action spectra of GT05-800 and P25 TiO_2 electrodes.

from −0.22 V (P25) to 0.08 V. Thus, the electronic interaction between graphit-like carbon and TiO_2 might cause an anodic shift of the valence band edge of TiO_2, which consequently results in the acceleration of oxidative interfacial electron transfer reactions.

X-ray absorption spectroscopy shows that the surface states in TiO_2 nanocrystallites are coordinately unsaturated Ti sites that are formed upon surface reconstruction of nanoparticles.[26] When surface Ti atoms of nanoparticles are coupled with organic molecules, e.g., enediol ligands (dopamine, etc.) or β-cyclodextrin, these undercoordinated surface sites will restructure into a more optimal octahedral structure.[27,28] In the case of GT05-800, the graphite-like carbon is able to surface conjugate (d-π conjugate) with the coordinately unsaturated Ti atoms in order to form an optimal structure. Based on this hybrid effect of TiO_2 and surface graphite-like carbon layers, the following photocatalytic mechanism under visible light irradiation is proposed: Graphite-like carbon absorbs visible light and the excited state electrons are subsequently injected into the conduction

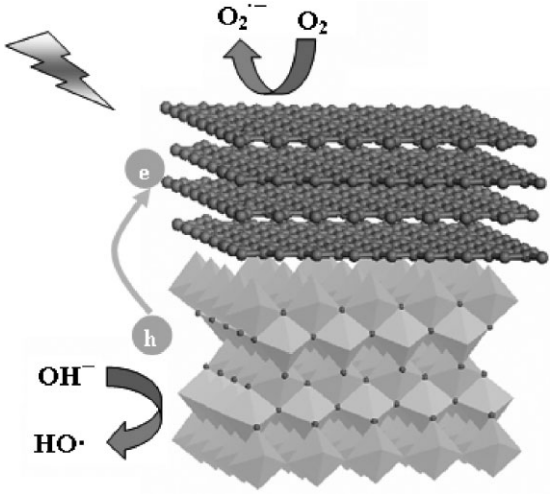

Scheme 2. Schematic drawing of TiO_2/graphite-like carbon (GT) composites.

band (*d*-orbital) of TiO_2 due to the *d*-π interaction. Then, the excited electrons are transfered to the surface where they react with oxygen to yield superoxide radicals, which later oxidize the FAD on the surface.

3. Conclusions

The mediating role of graphite-like carbon in storing and shuttling photogenerated electrons from the semiconductor to an acceptor in a photocatalytic process is realized by hybridizing TiO_2 with graphite-like carbon layers. The electronic contact between semiconductor and graphite-like carbon results in an efficient separation of electron-hole pairs which minimizes the energy-dissipating electron-hole recombination and subsequently leads to higher photocatalytic activity under UV irradiation. This approach of graphite-like carbon hybridization of TiO_2 also extends TiO_2's response into the visible range of the solar spectrum due to the electronic coupling between π states of graphite-like carbon and conduction band states of TiO_2.

4. Experimental

Synthesis of TiO_2/carbon nanoparticles: TiO_2 used to prepare TiO_2/carbon composite (GT) samples was obtained from Degussa (P-25 TiO_2). All other reagents were purchased as p.a. grade chemicals from Beijing Chemical Reagent Factory and used without further purification. Preparation of graphite-like carbon hybridized TiO_2 was realized in two steps. Firstly, 0.4 g P-25 TiO_2 and 0.5 g glucose were dissolved in 35 mL water assisted by ultrasonication until a clear solution was achieved. The solution was subsequently transferred to a 40 mL autoclave and hydrothermally treated at 180 °C for 4 h. Pure products were obtained after centrifugation at 5000 min^{-1} for 20 min. The subsequent cleaning process involved five cycles of centrifugation/washing/re-dispersion in water. The samples were collected via centrifugation and dried in an oven at 80 °C for 4 h.. Secondly, graphitization was achieved in a tube furnace by calcining at 800 °C for 3 h in N_2 flow (60 mL · min^{-1}). According to the experimental results, samples obtained exhibit a TiO_2@C core-shell structure, whereby the shell thickness depends on the amount of glucose used during synthesis.

Products naming: Products prepared with different amounts of glucose (0.1 g, 0.3 g, 0.5 g, 0.7 g, 0.8 g, 1.0 g, 4.0 g) and 800 °C calcinations temperature were named GT01-800, GT03-800, GT05-800, GT07-800, GT08-800, GT10-800, and GT40-800, respectively. While samples GT05-500, GT05-700, and GT05-800 represent products prepared with 0.5 g glucose at a calcination temperature of 500 °C, 700 °C, and 800 °C, respectively.

Analysis Techniques: X-ray diffraction (XRD) experiments were carried out using a Rigaku DMAX-2400 diffractometer with Cu K_α radiation. The average crystal size was determined from XRD pattern parameters according to the Scherrer equation (Eq. 3).

$$D_c = \frac{K\lambda}{\beta \cos\theta} \tag{3}$$

where D_c represents the average crystal size, K the Scherrer constant equal to 0.89, β the full width at half-maximum (FWHM), and θ the diffraction angle. The peak at 14.9 ° was used for the calculation of the crystal size, because it had a relatively strong intensity and did not overlap with any other diffraction peaks. The grain size was measured using a Hitachi H-800 transmission electron microscope (TEM), whereby the accelerating voltage of the electron beam was 200 kV. Raman spectra were acquired with a Raman microspectrometer (Renishaw 1000 NR) using an Ar ion laser (632.8 nm). Raman spectra were measured using a microscope equipped with a 20x objective which focused the incident excitation laser radiation into a spot 1–2 μm or 2–3 μm in diameter, respectively, and the scattered light was collected. The laser power was kept low enough to avoid heating of the samples. This was achieved by optical filtering and/or defocusing of the laser beam at the sample surface. Spectra were collected in the range of 1000–200 cm^{-1} with a resolution of 1 cm^{-1}. UV-vis diffuse reflectance spectra (DRS) were measured using Hitachi U-3010 UV-Vis spectrophotometer. TGA-DTA analysis was performed in air at a heating rate of 5 K · min^{-1} on a Dupont 1090 thermal analyzer.

Photochemical Experiments: The optical system for the photocatalytic reactions was composed of a 500 W Xenon arc lamp and a cutoff filter ($\lambda > 420$ nm). The average light intensity during the visible light experiments was 31 mW · cm^{-2}. A 400 mL cylindrical quartz vessel, which was equipped with an inlet, an outlet, and a sample port was used as photocatalysis reactor. In a typical process, 0.1 g photocatalyst was dispersed in about 1 mL ethanol. The solution was dripped onto a clean glass slide and spread to form a uniform film after which the photocatalyst was placed into the reactor. A mixture containing approx. 1800 ppm formaldehyde (FAD) was fed into the photoreactor which was subsequently seeled. The photocatalytic reaction was started by turning on the UV-lamp. Changes in FAD concentration within the sealed photoreactor were measured using a SP-502 gas chromatograph equipped with a flame ionization detector and a 2 m stainless steel column (GDX-403) at 373 K. UV light was provided by a 11 W UV-light lamp ($\lambda = 254$ nm, Institute of Electric Light Sources, Beijing). The distance between the film and the light source was 5 cm, where the light intensity was measured to be 120 mW · cm^{-2}.

P25 TiO_2 and GT electrodes preparation by dip-coating: Briefly, 5 mg of photocatalyst was suspended in 5 mL ethanol to produce a slurry, which was then dip-coated onto a 2 cm × 4 cm indium-tin oxide (ITO) glass electrode. Electrodes were exposed to UV light for 12 h to eliminate ethanol and subsequently calcined at 400 °C for 30 min under N_2 flow (rate = 60 mL · min^{-1}). Saturated calomel electrodes (SCE) and Pt gauze were placed in the reactor as working (collector), reference, and counter electrodes, respectively. Prior to and during all measurements, the electrolyte (0.5M Na_2SO_4) was purged with nitrogen. All investigated electrodes were of similar thickness (0.8–1 μm). Potentials are given with reference to the normal hydrogen electrode (NHE).

Received: December 17, 2007
Revised: February 26, 2008

[1] a) M. Kaneko, I. Okura, in *Photocatalysis*, (Eds: M. Kaneko, I. Okura), Kohdansha-Springer, Tokyo, Japan **2002**, pp. 1–5. b) T. Abe, M. Kaneko, *Prog. Polym. Sci.* **2003**, *28*, 1441.

[2] a) J. C. Crittenden, Y. Zhang, D. W. Hand, D. L. Perram, E. G. Marchand, *Water Environ. Res.* **1996**, *68*, 270. b) N. V. Muradov, *Sol. Energy* **1994**, *52*, 283.

[3] a) R. Asahi, T. Morikawa, T. Ohwaki, K. Aoki, Y. Taga, *Science* **2001**, *293*, 269. b) U. M. Shahed, A. Mofareh, B. William, *Science* **2002**, *297*, 2243. c) S. Sakthivel, H. Kisch, *Angew. Chem. Int. Ed.* **2003**, *42*, 4908. d) B. Kraeutler, A. J. Bard, *J. Am. Chem. Soc.* **1978**, *100*, 4317. e) P. V. Kamat, *Pure Appl. Chem.* **2002**, *74*, 1693.

[4] W Choi, *J. Phys. Chem.* **1994**, *98*, 13669.

[5] a) V. Subramanian, E. E. Wolf, P. V. Kamat, *J. Am. Chem. Soc.* **2004**, *126*, 4943. b) G. Burgeth, H. Kisch, *Coord. Chem. Rev.* **2002**, *230*,

41. c) M. Jakob, H. Levanon, P. V. Kamat, *Nano Letter.* **2003**, *3*, 353.
[6] a) S. H. Elder, F. M. Cot, Y. Su, S. M. Heald, A. M. Tyryshkin, M. K. Bowman, Y. Gao, A. G. Joly, M. L. Balmer, A. C. Kolwaite, K. A. Magrini, D. M. Blake, *J. Am. Chem. Soc.* **2000**, *122*, 5138. b) S. K. Poznyak, D. Talapin, A. Kulak, *J. Phys. Chem. B* **2001**, *105*, 4816.
[7] H. Hagiwara, N. Ono, T. Inoue, H. Matsumoto, T. Ishihara, *Angew. Chem. Int. Ed.* **2006**, *45*, 1420.
[8] H. G. Kim, P. H. Borse, W. Choi, J. S. Lee, *Angew. Chem. Int. Ed.* **2005**, *44*, 4585.
[9] M. C. Long, W. M. Cai, J. Cai, B. X. Zhou, X. Y. Chai, Y. H. Wu, *J. Phys. Chem. B* **2006**, *110*, 20211.
[10] a) W. Ma, C. Yang, X. Gong, K. Lee, A. J. Heeger, *Adv. Funct. Mater.* **2005**, *15*, 1617. b) M. Reyes-Reyes, K. Kim, D. L. Carrol, *Appl. Phys. Lett.* **2005**, 083506.
[11] a) S. Shanmugam, A. Gabashvili, D. S. Jacob, J. C. Yu, A. Gedanken, *Chem. Mater.* **2006**, *18*, 2275. b) Z. Lei, Y. Xiao, L. Dang, W. You, G. Hu, J. Zhang, *Chem. Mater.* **2007**, *19*, 477.
[12] a) W. J. Ren, Z. H. Ai, F. L. Jia, L. Z. Zhang, X. X. Fan, Z. G. Zou, *Appl. Catal. B: Environ.* **2007**, *69*, 138. b) C. K. Xu, R. Killmeyer, M. M. Gray, S. Khan, *Appl. Catal. B: Environ.* **2006**, *64*, 312.
[13] M. Inagaki, Y. Hirose, T. Matsunaga, T. Tsumura, M. Toyoda, *Carbon* **2003**, *41*, 2619.
[14] a) T. Oksaka, F. Izumi, Y. Fujiki, *J. Raman Spectrosc.* **1978**, *7*, 321. b) H. Berger, H. Tang, F. Kevy, *J. Cryst. Growth* **1993**, *130*, 108.
[15] a) S. P. S. Porto, P. A. Fbeury, T. C. Damen, *Phys. Rev.* **1967**, *154*, 522. b) Y. Hara, M. Nicol, *Phys. Status Solidi B* **1974**, *94*, 317.
[16] A. L. Bassi, D. Cattaneo, V. Russo, C. E. Bottani, E. Bartoriri, T. Mazza, P. Pisen, P. Midani, F. O. Ernst, K. Wegner, S. E. Pratsinis, *J. Appl. Phys.* **2005**, *98*, 74305.
[17] W. F. Zhang, Y. L. He, M. S. Zhang, Q. Chen, *J. Phys. D: Appl. Phys.* **2000**, *33*, 912.
[18] a) J. C. Parker, R. W. Sieger, *Appl. Phys. Lett.* **1990**, *57*, 943. b) J. C. Parker, R. W. Sieger, *J. Mater. Res.* **1990**, *5*, 1246.
[19] P. C. Eklund, J. M. Holden, R. A. Jishi, *Carbon* **1995**, *33*, 959.
[20] F. B. Su, X. S. Zhao, Y. Wang, J. H. Zeng, Z. C. Zhou, J. Y. Lee, *J. Phys. Chem. B* **2005**, *109*, 20200.
[21] F. Tuinstra, J. L. Koenig, *J. Chem. Phys.* **1970**, *53*, 1126.
[22] M. S. Wong, S. H. Wang, T. K. Chen, C. W. Weng, K. K. Rao, *Surf. Coat. Technol.* **2007**, *202*, 890.
[23] T. Tsumura, N. Kojitani, I. Izumu, N. Iwashita, M. Toyoda, M. Inagaki, *J. Mater. Chem.* **2002**, *12*, 1391.
[24] a) K. Y. Tse, B. M. Nichols, W. Yang, J. E. Butler, J. N. Russell, R. J. Hamers, *J. Phys. Chem. B* **2005**, *109*, 8523. b) F. Fabregat-Santiago, G. Garcia-Belmonte, J. Bisquert, P. Bogdanoff, A. Zaban, *J. Electrochem. Soc.* **2003**, *150*, E293.
[25] M. R. Hoffmann, S. T. Martin, W. Y. Choi, D. W. Bahnemann, *Chem. Rev.* **1995**, *95*, 69.
[26] A. Ishikawa, T. Takata, J. N. Kondo, M. Hara, H. Kobayaski, K. Domen, *J. Am. Chem. Soc.* **2002**, *124*, 13547.
[27] N. M. Dimitrijevic, Z. V. Saponjic, D. M. Bartels, M. C. Thurnauer, D. M. Tiede, T. Rajh, *J. Phys. Chem. B* **2003**, *107*, 7368.
[28] T. Tachikawa, S. Tojo, M. Fujitsuka, T. Majima, *Chem. Eur. J.* in press.